# Acoustic Liner Drag: Further Measurements on Novel Facesheet Perforate Geometries

Brian M. Howerton[1] and Michael G. Jones.[2]
*NASA Langley Research Center, Hampton, VA, 23681*

Christopher M. Jasinski.[3]
*University of Notre Dame, South Bend, IN, 46556*

**Over the past several years, the NASA Langley Liner Physics Team has worked to develop methods capable of characterizing the aerodynamic drag of acoustic liners in addition to their acoustic performance. For a given liner, one can compute its resistance factor, λ, based on static pressure drop measurements. The current study details experiments in the NASA Langley Grazing Flow Impedance Tube to quantify the relative drag of several perforate-over-honeycomb liner configurations at flow speeds of Mach 0.3 and 0.5. The liner facesheets incorporate novel perforate geometries rather than the conventional, round hole designs typically used. Measurements of the resistance factor for each liner are made with and without acoustic excitation. A tonal acoustic source is used at sound pressure levels of 140 and 150 dB over a frequency range of 400 to 3000 Hz when performing acoustic measurements. Educed impedance spectra are calculated to determine the impact of variations in perforate geometry on acoustic performance and the relationship between acoustic and drag performance.**

## Nomenclature

| | | |
|---|---|---|
| $a$ | = | duct width |
| $b$ | = | duct height |
| $c$ | = | speed of sound |
| $d_h$ | = | duct hydraulic diameter |
| $\gamma$ | = | ratio of specific heats |
| $\lambda_{L+SW}$ | = | resistance factor of the liner plus the hardwall portion of the test section |
| $\lambda_L$ | = | resistance factor of the liner |
| $\lambda_{SW}$ | = | resistance factor of a smooth wall sample |
| $LL$ | = | liner length |
| $M$ | = | centerline flow Mach number |
| $p_{s\infty}$ | = | static pressure, absolute |
| $p$ | = | static pressure, differential |
| $P_{atm}$ | = | atmospheric pressure |
| $P$ | = | perimeter length of the test section |
| $S$ | = | static pressure port separation distance |
| $q$ | = | dynamic pressure |
| $W_L$ | = | width of liner |
| $x$ | = | streamwise duct coordinate |
| $\rho$ | = | density |

[1] Research Scientist, Structural Acoustics Branch, MS 463, Senior Member AIAA, (brian.m.howerton@nasa.gov).
[2] Senior Research Scientist, Structural Acoustics Branch, MS 463, Associate Fellow AIAA.
[3] Ph.D Graduate Student, Aerospace and Mechanical Engineering Department, (chrismjasinski@gmail.com).

American Institute of Aeronautics and Astronautics

# I. Introduction

Fuel efficiency has been a significant concern for airframers and engine companies developing commercial aircraft products over the last 40 years. Regulatory pressures in other areas besides performance have led to design compromises that trade fuel efficiency for compliance with noise constraints. Acoustic liners have been successfully applied to reduce the radiated noise created by turbofan engines, but with a weight and drag penalty that increases fuel burn. Over the past several decades, research efforts in acoustic liners have mainly focused on understanding liner physics and how to optimize liner impedance (whether uniform or variable) to achieve maximum noise reduction. This work could be applied to reduce the amount of required treatment that, when coupled with advancements in liner materials and manufacturing, would mitigate some of the weight penalty. Recently, research into lowering liner drag by modification of the facesheet has shown some promise. The majority of acoustic liners developed for production aircraft engines use a facesheet perforated with round holes (Fig. 1) to provide the necessary porosity. Reducing the hole diameter while keeping the total percent open area (POA) constant has been shown to reduce liner drag.[1] Changing the perforate geometry and orientation, relative to the flow, may create a configuration with improved drag performance.
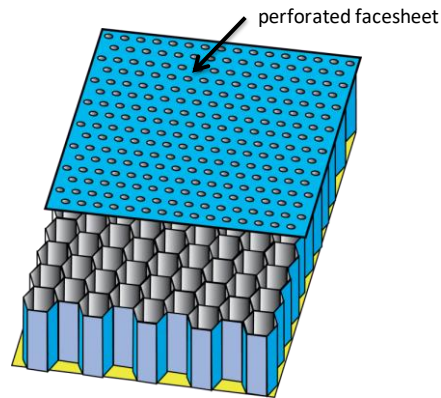


**Figure 1. Conventional liner construction.**

Howerton and Jones[2] evaluated several alternate perforate geometries and discovered a slot geometry, oriented with the long axis perpendicular to the flow, that significantly reduced the measured liner resistance factor ($\lambda$). This new geometry cut the penalty between a smooth wall and a conventional, round-hole perforate by ~50% without detrimental effect on the liner's acoustic performance (Fig. 2).
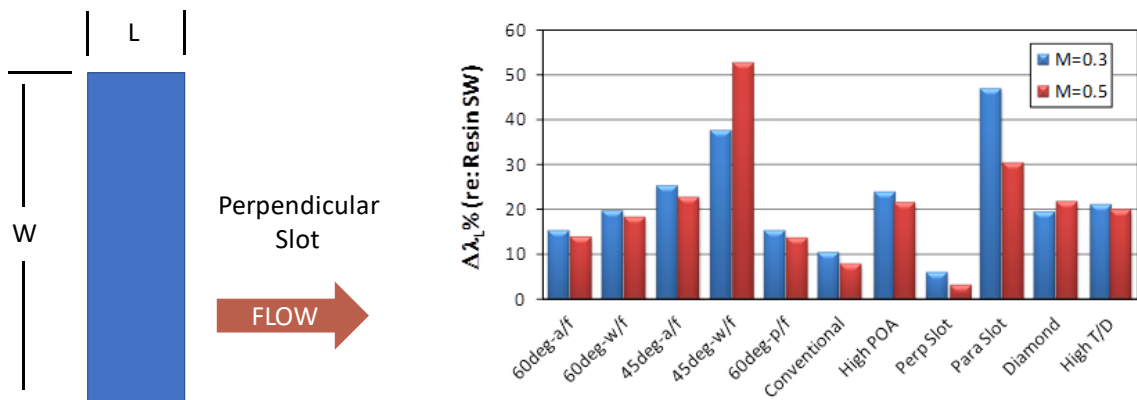


**Figure 2. Perpendicular slot geometry and a comparison of reductions in resistance factor for various liner facesheet perforates.**

The purpose of the current investigation is to evaluate the effects of perforate geometry and orientation on the drag with a number of novel facesheet perforate configurations. In many aspects, it is a continuation of Ref 2 as an experimental study to identify perforates that may provide drag benefits superior to the aforementioned

2

perpendicular slot. Each liner is tested in the NASA Langley Research Center Grazing Flow Impedance Tube (GFIT) at flow speeds of Mach 0.3 and 0.5. The resultant acoustic and aerodynamic responses are compared to (1) determine if any designs provide reduced drag, and (2) determine the impact of these perforate geometries on the acoustic performance of the liner. Details are provided on the static pressure drop method used to compute $\lambda$ along with a description of the liner samples tested. Later sections show these results for various perforate geometries with and without acoustic excitation. Data are presented on liner acoustic performance focusing on the educed impedances. Interactions between acoustic performance and liner drag are also discussed.

## II.  Liner Drag Measurements

As in previous drag studies using the GFIT, the drag of each configuration, relative to a smooth wall, will be determined by measuring differences in the static pressure drop along the duct wall opposite of the liner sample. Similar to the approach of Nikuradse when studying roughness in pipes[3], this method can be applied to small ducts with fully-developed, turbulent flow. From the static pressure data and selected flow parameters, one can compute the duct resistance factor, $\lambda$ (also known as the 'friction factor'), given by the equation:

$$\lambda = \frac{dp}{dx}\frac{d_h}{q}$$

( 1 )

where the hydraulic diameter of the flow duct ($d_h$) can be written as:

$$d_h = \frac{2ab}{a+b}$$

( 2 )

and the compressible form for q is given by:

$$Q = \frac{\gamma}{2}p_{s\infty}M^2$$

( 3 )

The nondimensional nature of $\lambda$ allows the static pressure data to be normalized, taking out the effects of duct Mach number and static pressure variations between runs. Note that $\lambda$ encompasses the sum of both the skin friction and pressure components of drag. Thus, any effects of the liner cavity are also included, thereby differentiating this method from others that are solely measuring skin friction. The results of these calculations can be used to provide a relative measurement of drag between liner configurations.

## III.  Experiment

The experimental investigation involves testing of seven liners and one smooth wall configuration in the GFIT. Each facesheet is 3D printed using a stereolithography process whereby liquid plastic resin is photopolymerized using laser light to build the facesheet in layers. The perforations result when areas of the facesheet are not subjected to the light. The sheets are post-processed to sand the flow side smooth. A resin smooth wall sample (RSW) with no perforations is included to provide a reference baseline. All facesheets were constructed to have a percent open area (POA) of eight. For each configuration, a high-accuracy measurement of the axial static pressure drop across the liner is made to compute the liner resistance factor with and without acoustic excitation. Simultaneously, the acoustic performance of each liner is characterized using measurements made with an array of microphones surrounding the liner sample.

### A.  Liner Facesheet Construction

For this investigation, several perforate geometries are variations of slot geometries that built upon the results from Howerton and Jones.[2] Further samples using a simplified teardrop shape were also printed with orientations where the long axis is both parallel and skewed 45 degrees to the flow direction. A facesheet using the perpendicular slot previously constructed for Ref. 2 is included for comparison. Details of the perforate shapes and dimensions are provided in Figure 3. The angled configurations are intended to induce a spanwise velocity to the flow while the two chevron perforates are an attempt to create longitudinal vorticity similar to the riblet low-drag treatments studied by various entities. A teardrop shape also seemed a logical choice to investigate with this version simplified as the combination of a semicircle and an equilateral triangle of common dimension. Where applicable,

American Institute of Aeronautics and Astronautics

some of the configurations are tested in the orientation as shown in Figure 3 (with a -D designation signifying that it is pointing downstream) and again in a reversed orientation (-U designation) to determine the effects of relative flow direction.
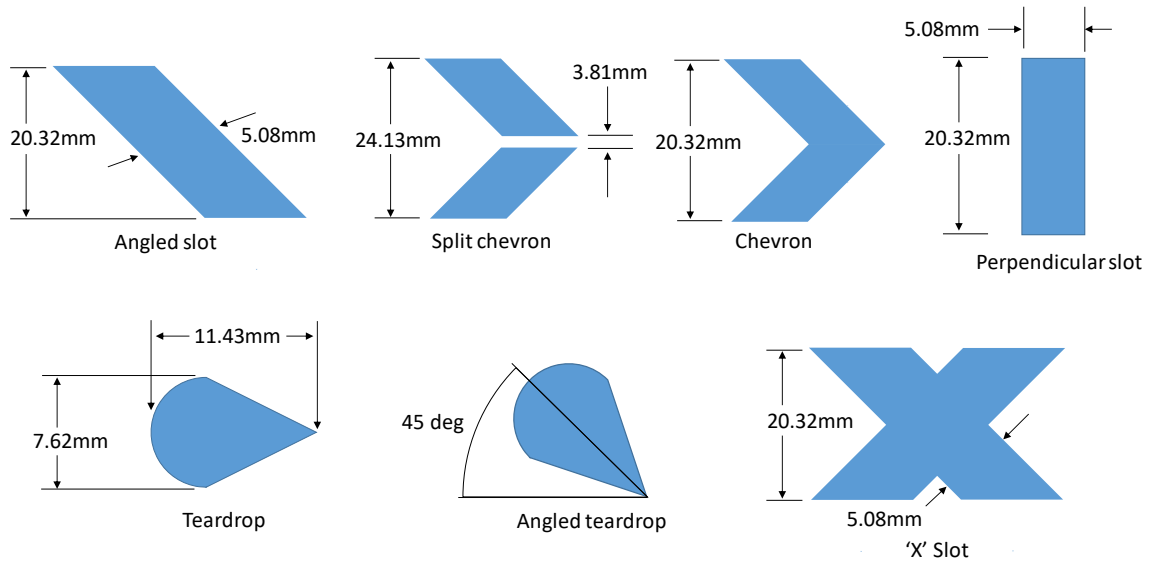


**Figure 3. Facesheet perforate geometry (not to scale).**

## B. Liner Core Construction

Each facesheet was mounted onto a metallic liner core with a cavity depth of 38.1 mm. The liner core is from a previous investigation that was repurposed for this experiment. To allow for rapid changes of liner configuration, the facesheets are not bonded to the core structure but clamped by their long edges as part of installation in the test rig. Note that the core is constructed for the full length of the GFIT test window (614.4 mm) while the facesheets are only 460.8 mm long. An aluminum filler blank was fabricated to cover the remaining portion of the core. Figure 4 shows a typical arrangement with the filler blank (right) and the facesheet (left) overlaid on the core.
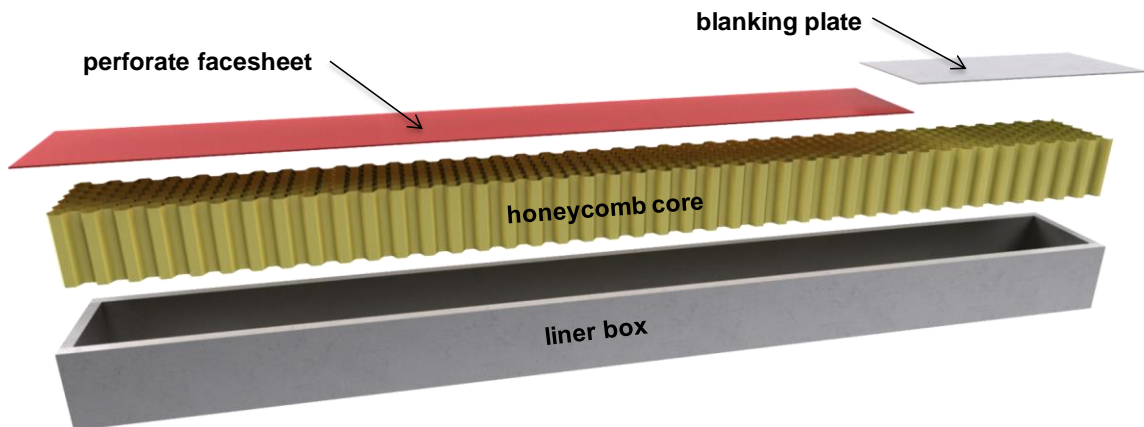


**Figure 4. Typical liner sample.**

American Institute of Aeronautics and Astronautics

## C.  Grazing Flow Impedance Tube (GFIT)

The NASA Langley GFIT facility is routinely used to determine the acoustic characteristics of noise reduction treatments (acoustic liners) for aircraft jet engine nacelles and nozzles. With the addition of some high-accuracy pressure instrumentation, however, calculations can be made of liner friction factors to evaluate drag performance. The facility is a wind tunnel with a 50.8 mm by 63.5 mm rectangular cross section. The flow path (Fig. 5) consists of a straight duct with an upstream acoustic source section using 12 drivers, interchangeable lengths of blank duct, a test section where the liner sample is held along the upper wall of the duct and an array of 95 measurement microphones leading to a 6-driver downstream source section (not used for this study). Near-anechoic terminating diffusers are employed at each end of the duct to control reflections and reduce overall flow noise. The source sections can generate sound pressure levels up to 150 dB for the frequency range between 400 and 3000 Hz. For flow, pressurized, heated air is supplied to the entrance of the GFIT while a vacuum system is used at the duct exit to 'pull' the flow out of the tube. The static pressure at the test section can thus be held to be near ambient at all flow velocities while also creating an adiabatic wall condition. Grazing flow velocities from Mach 0.0 to Mach 0.6 are available with such an arrangement.
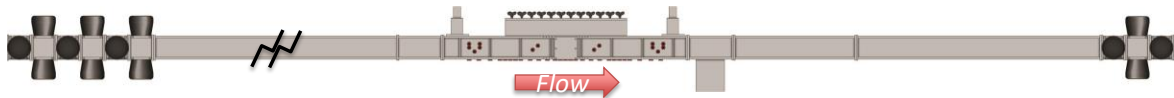


**Figure 5. Sketch of the NASA Langley Grazing Flow Impedance Tube (GFIT).**

Along the lower wall of the GFIT duct are 80 static pressure ports to measure the axial pressure distribution. A pair of those ports, separated axially by 1.07 m, bracket the test section liner opening and are used in the pressure drop measurement. They are connected to a high-accuracy, differential pressure gauge to measure the static pressure drop between these two locations. The gauge has a 0-6900 Pa range and 0.01% FS accuracy sampling at a rate of 10 Hz. A plot of the static pressure distribution in the test section for a smooth wall configuration at Mach 0.5 is given in Figure 6. The relative location of the liner and the ports used to compute the static pressure drop ($\Delta p$) are given in a sketch of the test section included above the plot. The measurement points are designated as Port 37 and Port 59, respectively.
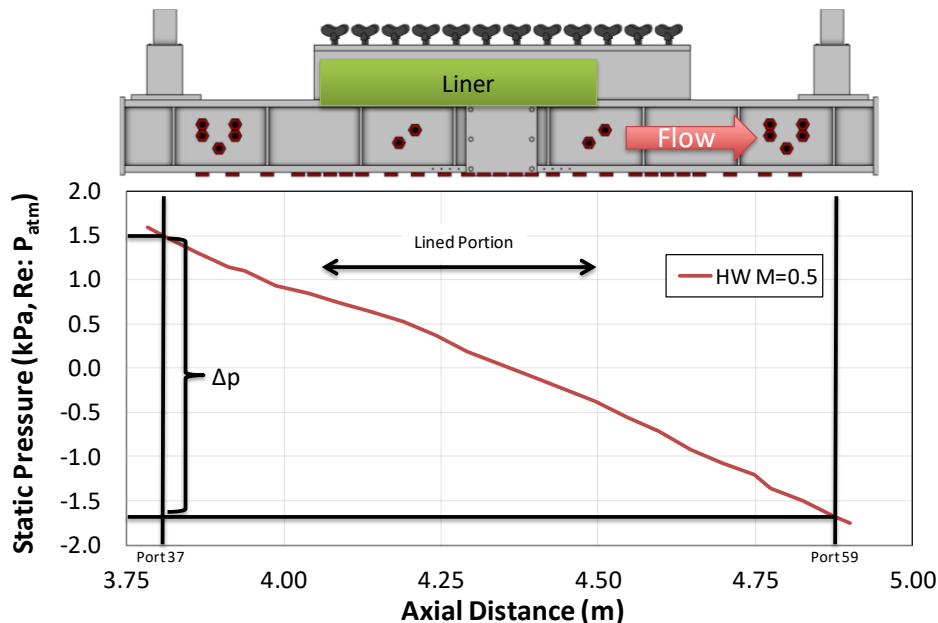


**Figure 6. GFIT Test Section Static Pressure Distribution, Smooth hardwall wall sample, Mach 0.5.**

American Institute of Aeronautics and Astronautics

## D.  Measurement Process

The measurement process follows the method used by Howerton and Jones[2] where averaged static pressure measurements are made for each configuration with no acoustic excitation at Mach 0.3 and 0.5. For each data set, 300 readings are acquired from the pressure gauge to provide the static pressure drop across the length of the liner. The target Mach number is held to a tolerance of +/- 0.002 while static pressure in the test section is set within +/-130 Pa in all cases. Tunnel conditions, including average Mach number and static pressure, are also recorded to allow computation of λ from Eq. (2).

From Ref. 2, the resistance factor for the lined portion of the duct can be given by:

$$\frac{\lambda_L}{\lambda_{SW}} = 1 + \frac{P}{W_L}\frac{S}{LL}\left(\frac{\lambda_{L+SW}}{\lambda_{SW}} - 1\right) \qquad (4)$$

where Figure 7 provides a sketch of the GFIT test section showing typical liner placement and various pertinent dimensions required to evaluate this expression.
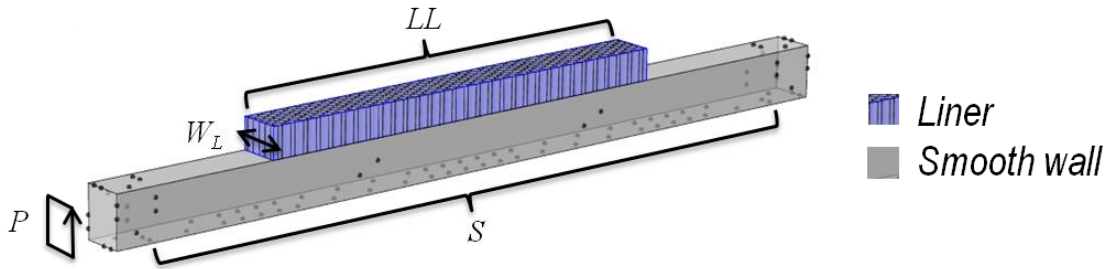


**Figure 7. Sketch of GFIT test section with dimensions used for liner drag eduction.**

Tonal acoustic excitation was also used at flow speeds of Mach 0.0 and 0.3 for frequencies between 400 and 3000 Hz (200 Hz increments) at a *target* sound pressure level (SPL) of 140 and 150 dB (re: 20 μPa). Previous experiments in the GFIT have used a single, fixed reference microphone to provide feedback for setting the sound pressure level. This choice led to frequency-dependent variations in level at the liner leading edge as the acoustic standing wave shifts relative to that microphone. An alternative strategy is now employed whereby the group of microphones located +/- 76.2 mm from the liner leading edge are surveyed for the maximum SPL value within the group. This value is used as feedback for setting the SPL and seems to provide a more consistent level at the liner leading edge across the frequency range. Static pressure measurements and acoustic surveys are performed simultaneously to evaluate the effect of acoustic excitation on liner drag. Data from the microphone array are used to compute the SPL and relative phase at the 95 microphone locations for each acoustic test point. The acoustic measurements allow for comparison of liner impedances educed using these data and the Straightforward Method of Watson.[4]

## IV.  Results and Discussion

### A.  Static Pressure Measurements

Figure 8 shows the liner resistance factor ($\lambda_L$, computed from Eq. (4)) for the smooth wall and five of the twelve liner configurations tested at Mach numbers of 0.3 and 0.5 with no sound. As expected, the smooth wall (RSW) configuration produces the lowest resistance factor with a decrease as the Mach number increases. Results from the perforates show the original Perpendicular Slot (Perp Slot) configuration to have lower drag than the new designs developed for this study. For all perforate cases, $\lambda_L$ increases with increasing Mach number and all configurations produce a drag penalty relative to the RSW. The overall values of $\lambda_L$ for the slot-based configurations are very similar although the variation with Mach number for the Chevron-U, Split Chevron-U and 'X' samples seems to be more pronounced. Also notable is the relatively poor performance of the teardrop-based samples which exhibit much higher resistance factor values, although angling the teardrop reduces the penalty

American Institute of Aeronautics and Astronautics

somewhat. Orientation of the perforate relative to the flow does seem to have an effect on the facesheet resistance factor. For all cases save for the Chevron geometry, having the pointed end of the perforate (the -U orientation) aimed upstream reduces the measured resistance factor values. The effect is most pronounced for the teardrop configurations.
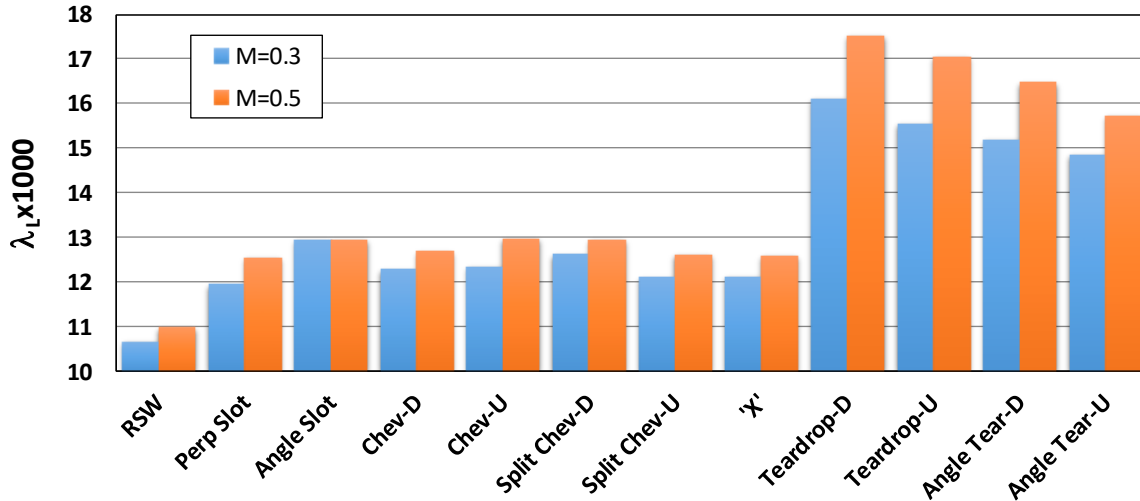


**Figure 8. Liner resistance factor ($\lambda_L$) x 1000 for Mach 0.3 and 0.5, no sound.**

### B. Resistance Factor Uncertainty

Previous studies by the authors using this measurement method produced results where the effect of different perforate configurations was easily discernable from resistance factor variation. Successive measurements for a configuration exhibited very little scatter with error estimates well below the differences observed between configurations. Given the relatively minor differences between the slot-based facesheet configurations in the current study and plans for an upcoming parametric investigation of perpendicular slot variations, further effort was put into quantifying and understanding the uncertainty in resistance factor measurements. The results are intended to guide efforts to reduce this uncertainty.

Using the RSW and Perp Slot facesheets, a test was performed to generate the necessary data for a statistical analysis of the liner resistance factor measurement. Each liner was alternatingly tested in the GFIT at Mach 0.5 with no sound. Eleven runs were made with five measurements (trials) acquired for each run. The twenty-two runs were performed over two successive days where there was some variation in atmospheric conditions. Logs of the GFIT operating parameters were acquired simultaneously with the pressure data for the $\lambda_L$ calculation for each trial. The results were analyzed to compute 95% confidence intervals for $\lambda_L$ and determine any trends relative to the measured parameters.

American Institute of Aeronautics and Astronautics

Figure 9 shows the measured resistance factors for the RSW and slot-based configurations with error estimates. Note that the estimate for the Perp Slot has been applied to the other slot configurations for convenience. From this result, one can see enough overlap between slot configurations as to make claims of variation between them statistically dubious.
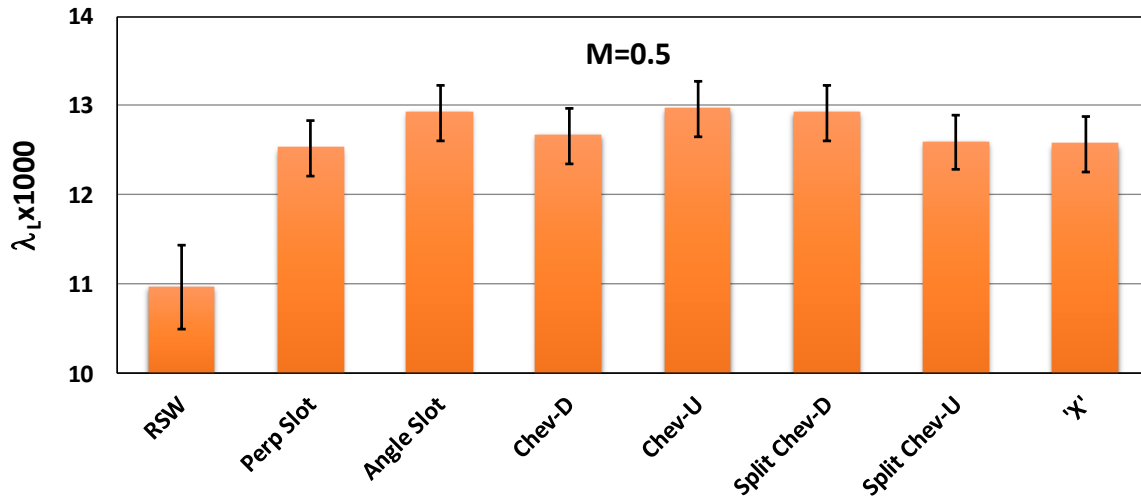


**Figure 9. Comparison of selected configurations with error estimates, Mach 0.5.**

In order to understand these estimates and the underlying causes of the measurement's variability, Figure 10 shows the variation in resistance factor for each trial. The results depict evidence of clustering in groups relative to when they were acquired (especially for the RSW configuration). Each trial requires approximately 3 minutes to record while a run of five trials lasts for approximately 30 minutes. Since the runs are interleaved between the two samples, there is generally an hour between each run for a particular sample. Each day had two data collection sessions (an AM and PM session) separated by a break of 1-2 hours.
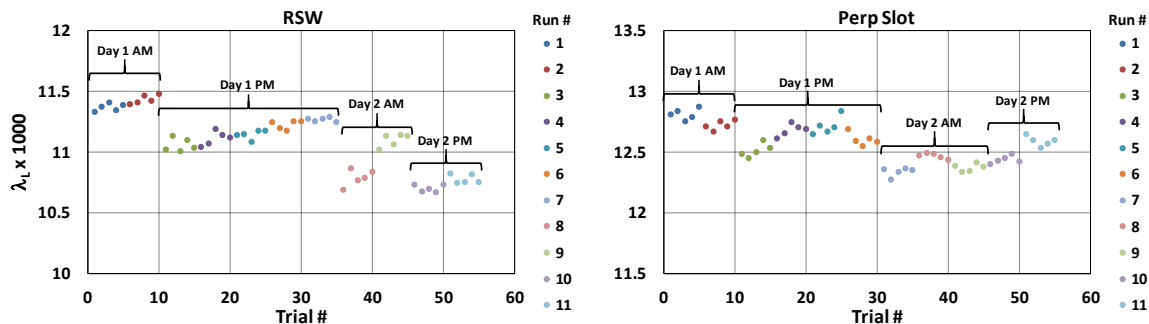


**Figure 10. Variation in resistance factor ($\lambda_L$) x 1000 with trial #, Mach 0.5.**

The RSW data shows a trend toward increasing $\lambda_L$ during each collection session while such a trend is not as easily discernable for the Perp Slot. The repeatability within a given run or even for a collection session is good, but the shifts between sessions negatively affect the computed error estimate. As stated previously, logs of the GFIT operating parameters are acquired simultaneously with the drag data and analyzed to see if any of them correlate with the behavior observed in resistance factor. The goal of such analysis is to find a means to normalize this variability out of the process or alter the test method to reduce these effects.

American Institute of Aeronautics and Astronautics

Figure 11 is a plot of GFIT static pressure (computed from the measured total pressure and isentropic relations) for each trial. Note that for a given run (five trials per run) the temperature generally increases. This increase results from efforts to maintain an adiabatic wall condition as prescribed for the impedance eduction method mentioned previously. The flow in the GFIT heats the walls, and thus, raises their static temperature which requires further increase in the flow temperature to compensate. The overall trends with this parameter generally follow the behavior of the resistance factor plots in Figure 10 indicating a correlation. Similar behavior can be seen in other GFIT temperature data.
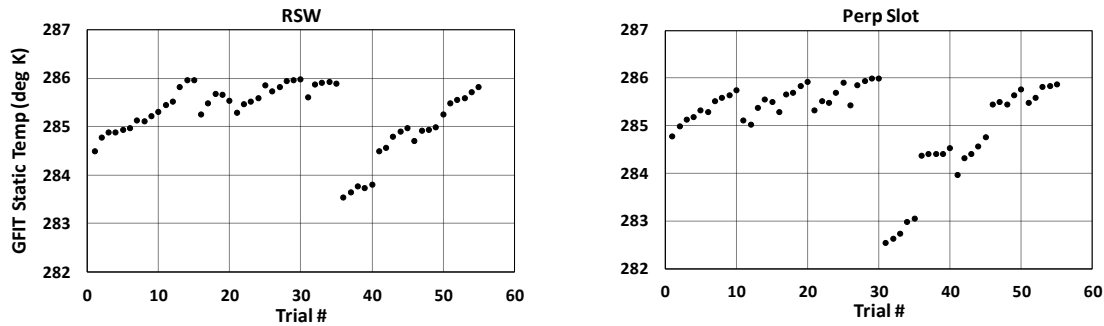
**Figure 11. Variation in GFIT static temperature with trial #, Mach 0.5.**

Furthermore, decreases in GFIT static pressure seemed to generally correlate with decreases in the calculated $\lambda_L$ as shown in Figure 12. For this plot, the five results for a given trial are averaged for each point. A linear fit to the resulting data is overlaid for both facesheet configurations. While the trend is similar, there are differences in slope that warrant further study.
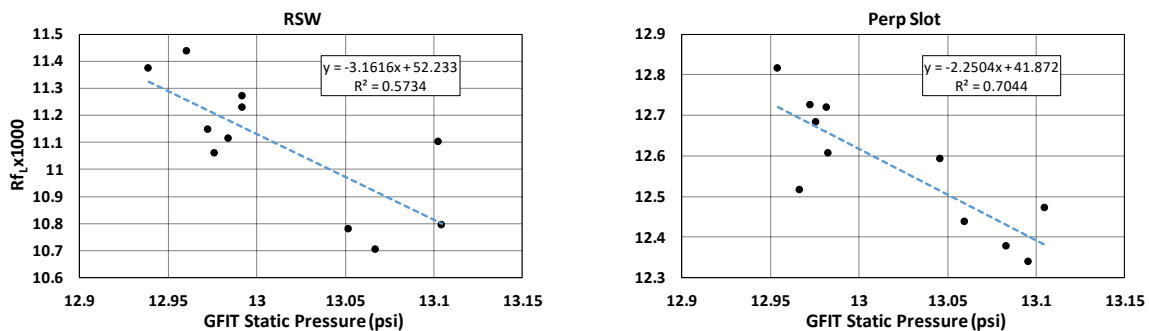
**Figure 12. Variation in liner resistance factor ($Rf_L$x1000) with GFIT static pressure, Mach 0.5.**

Other parameters such as Reynold's Number, flow velocity, atmospheric pressure, etc. either exhibited random variation or displayed trends incongruent with the resistance factor.

## C. Effects of Acoustic Excitation on Drag

Each liner configuration was evaluated in the presence of acoustic tonal excitation at target total SPLs of 140 and 150 dB. Frequencies ranged from 400 Hz to 3000 Hz, in 200 Hz increments. It was postulated prior to the test that the oscillatory motion of fluid through the facesheet perforations would affect the measured resistance factor. Expectations of significant variation in $\lambda_L$ at or near the frequencies of resonance (~1800-2200 Hz for these configurations) was also theorized. Figure 13 shows resistance factor spectra for Mach 0.3 and two SPLs. Several trends emerge from these plots. The resistance factor of the liner can vary with frequency and the variation increases with increasing SPL. Although not shown here, the authors have noted in Ref. 2 a decrease in the acoustic effects with increasing Mach number.

At Mach 0.3 with 150 dB excitation, there is an increase in the resistance factor for all perforate cases near 2000 Hz, which will be shown later to correspond to the resonance condition. The Perpendicular Slot configuration had the lowest values for resistance factor in all cases mirroring the results obtained with no sound. Of note is the

near identical behavior of the slot-based configurations with minimal differences observed even at the highest sound pressure level. Based on the results for the no-sound measurements, it is not unexpected for the teardrop configurations to have the highest values of resistance factor. These facesheets do trend towards lower values of $\lambda_L$ as the acoustic frequency increases. Furthermore, exposure to acoustic excitation does not seem to alter the rank order of these four configurations.
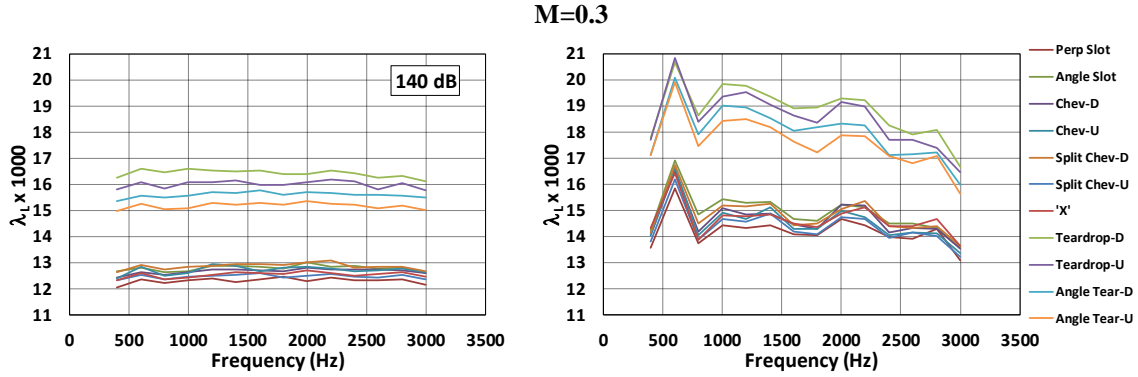
**M=0.3**



**Figure 13. Variation of resistance factor with acoustic excitation.**

### D. Acoustic Measurements

For each liner configuration, full acoustic pressure profiles were acquired at Mach 0.0 and 0.3 for the purposes of impedance eduction and evaluation of attenuation performance. These educed impedance spectra are compared to determine variations in liner acoustic performance relative to the parameters of the liner configuration.

Figure 14 shows the normalized impedance spectra (all impedances are normalized by $\rho c$) for the Perp Slot configuration for Mach 0.3 at 140 and 150 dB. The effect of increasing the SPL on the educed impedances is minimal for all configurations. Thus, for the sake of brevity, only the 140 dB spectra will be presented for the remaining configurations. Figures 15-20 present similar data for the remaining configurations. The general shape of the spectra are similar for all cases although the Perp Slot facesheet reaches resonance at a slightly lower frequency of ~1800 Hz as compared to the ~2000 Hz value for the remaining samples. Resistance is relatively flat across the frequency range while reactance exhibits a $-cot(kl)$ behavior ($k$ = freespace wavenumber, $l$ = cavity depth).
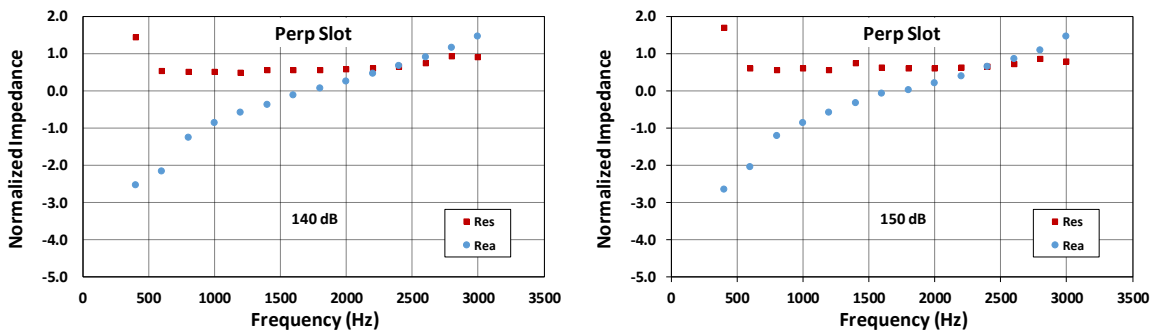


**Figure 14. Normalized impedance spectra for the Perpendicular Slot configuration, M=0.3.**

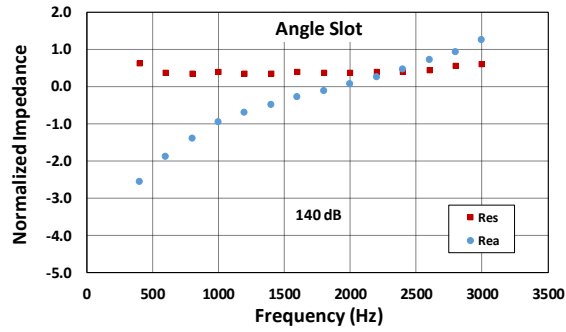American Institute of Aeronautics and Astronautics

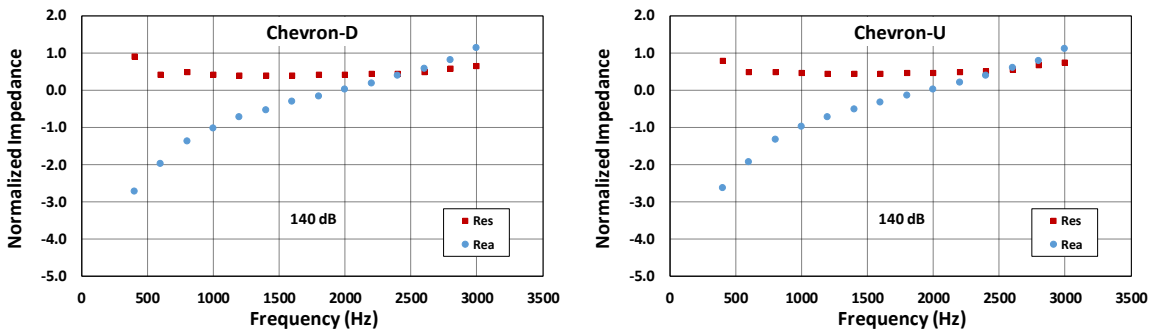**Figure 15. Normalized impedance spectra for the Angled Slot configuration, Mach 0.3, 140 dB.**



**Figure 16. Normalized impedance spectra for the Chevron-D (pointed downstream) and Chevron-U (pointed upstream) configurations, Mach 0.3, 140 dB.**
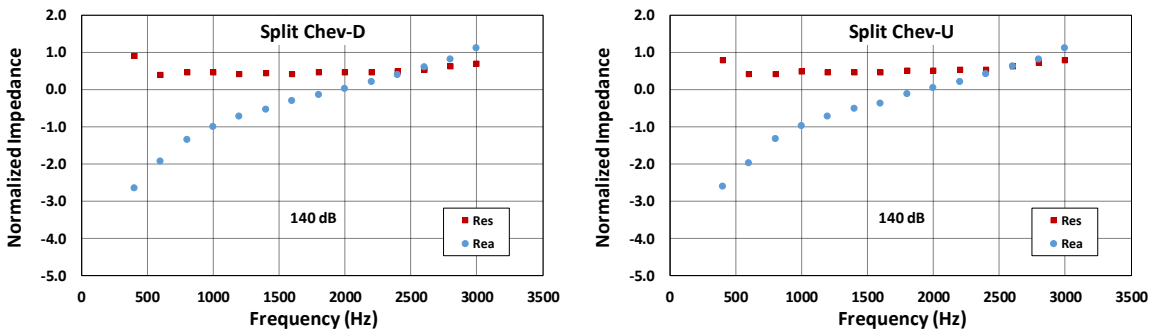


**Figure 17. Normalized impedance spectra for the Split Chevron-D (pointed downstream) and Split Chevron-U (pointed upstream) configurations, Mach 0.3, 140 dB.**
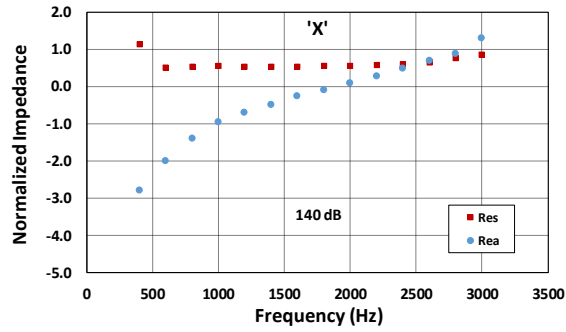
11

American Institute of Aeronautics and Astronautics

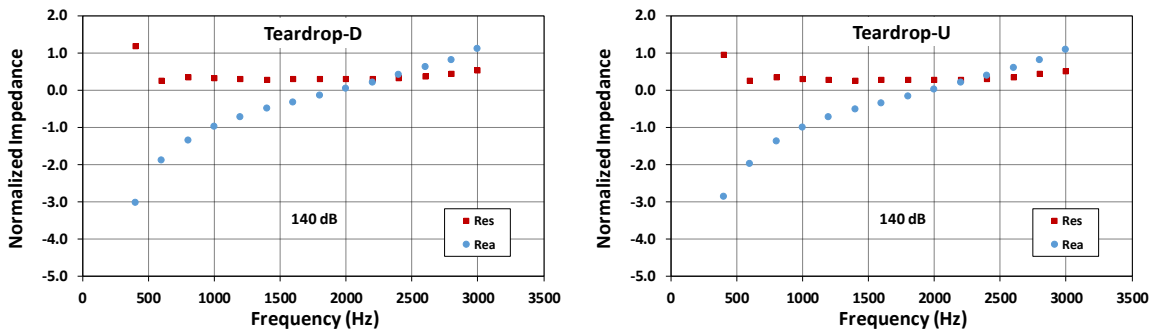**Figure 18. Normalized impedance spectra for the 'X' configuration, Mach 0.3, 140 dB.**



**Figure 19. Normalized impedance spectra for the Teardrop-D (pointed downstream) and Teardrop-U (pointed upstream) configurations, Mach 0.3, 140 dB.**
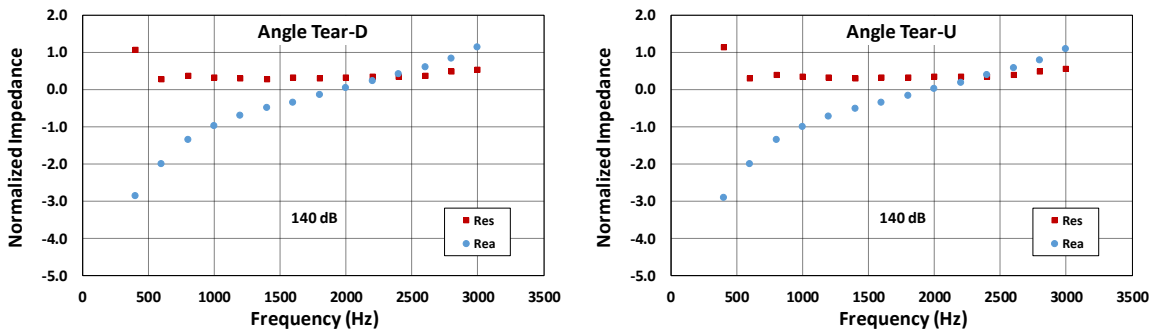


**Figure 20. Normalized impedance spectra for the Angled Teardrop-D (pointed downstream) and Angled Teardrop-U (pointed upstream) configurations, Mach 0.3, 140 dB.**

12

Figure 21 combines all the impedance spectra for each configuration for the case of Mach 0.0 and 140 dB excitation. The nominal value for resistance across all configurations is approximately $0.10\rho c$ across much of the frequency range with some spread between the curves near the extremes. Reactance spectra are very similar for all configurations with a slight steepening of the curve, as frequency increases, for the Perp Slot and 'X' configurations.
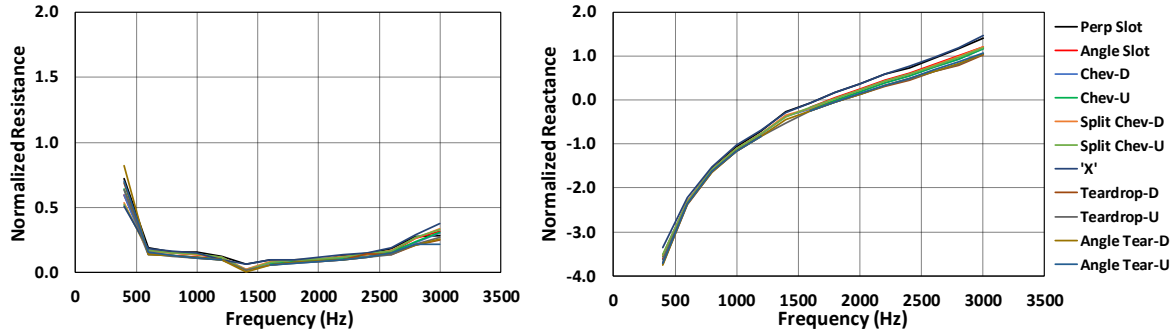


**Figure 21. Comparison of impedance spectra for all liners, Mach 0.0, 140 dB.**

Figure 22 plots similar data for the case of Mach 0.3 and 140 dB excitation. It is apparent that the perpendicular slot facesheet has a higher measured resistance spectrum as compared to most of the other configurations. The slot-based facesheets vary by approximately $0.25\rho c$ across the frequency range which is significantly more than observed for the no-flow condition. Since all facesheets were designed to the same POA and resistance was relatively invariant with configuration for Mach 0.0, this result would indicate that perforate geometry has an effect on liner impedance in the presence of grazing flow. The lowest resistance values correspond to the teardrop configurations.
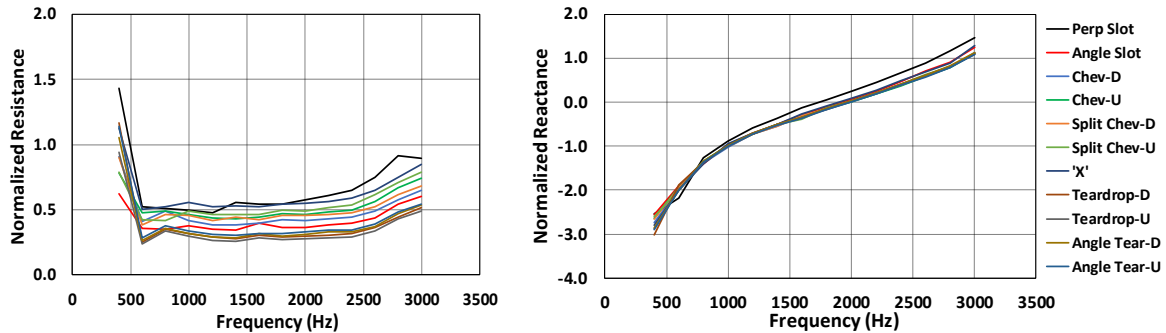


**Figure 22. Comparison of impedance spectra for all liners, Mach 0.3, 140 dB.**

### E.    Acoustic/Drag Interactions

This section will focus on observations related to the measured liner resistance factors as they relate to the acoustic impedance spectra. A comparison of the normalized acoustic resistance and the resistance factor spectra can be seen in Figure 23. Previous experiments[2] have shown that increasing facesheet resistance generally results in lower values of $\lambda_L$. The current results agree with that conclusion as well with the Perp Slot configuration exhibiting the highest nominal resistance and the lowest nominal values for resistance factor. Other slot configurations, such as the Angle Slot, have lower resistances and thus higher values of $\lambda_L$. Configurations based on the teardrop geometry were shown previously to produce the most drag and have the lowest corresponding values for resistance. This trend has been so pervasive in this and earlier studies, that it might be possible to rank order liner designs by acoustic results alone if the differences in resistance factor between configurations are statistically significant. Such a 'rule of thumb' could be useful to the acoustic community to evaluate relative drag in the absence of the specialized measurement techniques used here and by others.
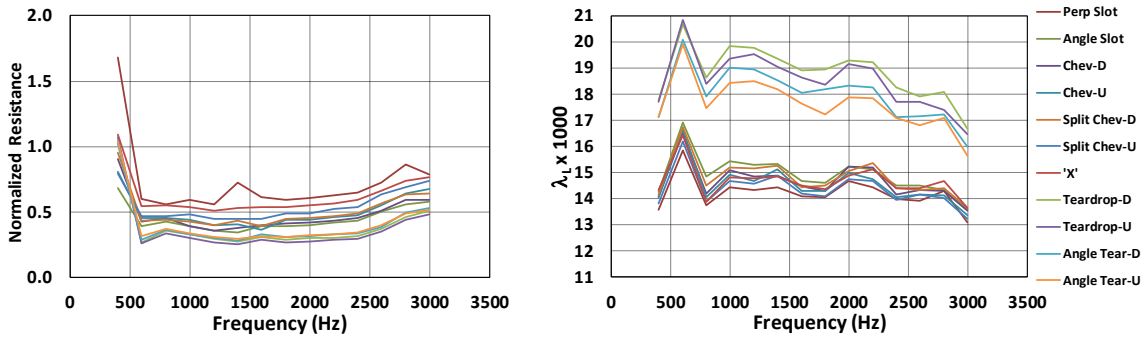
American Institute of Aeronautics and Astronautics

**Figure 23. Comparison of normalized impedance spectra and the corresponding $\lambda_L$ for all liners, Mach 0.3, 150 dB.**

## V.  Concluding Remarks

Measurements of liner resistance factors were made for eight liner configurations employing non-round hole perforations and a smooth wall baseline for flow Mach numbers of 0.3 and 0.5. The effects of acoustic excitation on $\lambda_L$ for two sound pressure levels were also investigated. Analysis of the acoustic data was performed to educe liner impedance spectra. The results were compared to the drag data in an effort to understand general trends related to these novel facesheet perforate designs. Several observations were noted:

1. All of the slot-derived novel perforate designs produced statistically similar resistance factor values as compared to the previously tested perpendicular slot configuration although the perpendicular slot was the lowest. No configuration was better than the smooth wall.

2. All of the teardrop based perforate designs exhibited significantly higher values for $\lambda_L$ relative to the perpendicular slot design.

3. For configurations tested in their alternate orientation, the upstream configuration generally produced lower resistance factor values.

4. Statistical analysis of multiple drag measurements for two of the configurations provided error estimates for $\lambda_L$. Correlations between resistance factor, GFIT static temperature and static pressure were noted.

5. Variation of resistance factor with acoustic excitation increased with increasing SPL and decreased with increasing Mach number.

6. The educed impedance spectra for the various perforates developed for this study were very similar to each other for the Mach 0.0 condition. At Mach 0.3, greater variation in resistance spectra was noted for the slot based configurations while teardrop facesheets had lower acoustic resistance. The perpendicular slot geometry had higher resistance and generally higher reactance values.

7. Perforate shape can have an effect on acoustic resistance in the presence of grazing flow. For this investigation, the slot geometries had higher resistance values than the teardrop designs.

8. Generally, lower drag configurations will have higher acoustic resistance.

## Acknowledgments

American Institute of Aeronautics and Astronautics

# References

[1]Howerton, Brian M., and Jones, Michael G., "Acoustic Liner Drag: A Parametric Study of Conventional Configurations," AIAA Paper 2015-2230, 21st AIAA/CEAS Aeroacoustics Conference, AIAA Aviation 2015, June 2015.

[2]Howerton, Brian M., and Jones, Michael G., "Acoustic Liner Drag: Measurements on Novel Facesheet Perforate Geometries," AIAA Paper 2016-2979, 22nd AIAA/CEAS Aeroacoustics Conference, June 2016.

[3]Nikuradse, J., "Laws of Flow in Rough Pipes," NACA TM-1292, November 1950.

[4]Watson, W. R., and Jones, M. G., "A Comparative Study of Four Impedance Eduction Methodologies Using Several Test Liners," AIAA Paper 2013-2274, 19th AIAA/CEAS Aeroacoustics Conference, May 2013.

American Institute of Aeronautics and Astronautics